Proceedings of the 13th International Workshop on Discrete Event Systems, Xi'an, China, May 30 - June 1, 2016

A Resiliency Measure for Electrical Power Systems

Mariam Ibrahim[1&2], *Member, IEEE*, Jun Chen[1], *Member, IEEE* and Ratnesh Kumar[1], *Fellow, IEEE*
[1] Iowa State University, Dept. of Elec. & Comp. Eng., Ames, IA 50011.
[2] German Jordanian University, Dept. of Mechatronics Eng., Amman 11180, Jordan.
Emails: {mariami,rkumar}@iastate.edu, jchenee2015@gmail.com.

***Abstract*— Providing a resiliency measure for power systems is one of the challenges towards its Dynamic Security Assessment. This paper introduces a resiliency measure, called *Level-of-Resilience* (LoR), determined by examining: (i) the *Region-of-Stability-Reduction* (RoS_R), as the RoS evolves under attack and recovery actions as captured by a "*modal-RoS*", (ii) the eventual *Level-of-Performance-Reduction* (LoP_R), as measured by percentage of reduction of load served, and (iii) *Recovery-Time (RT)*, which is the time system takes to detect and recover from an attack or a fault. We illustrate our measure by comparing resiliency level of two power systems under two different attack scenarios.**

I. Introduction

Resiliency can be defined as "*ability to withstand adverse events*". Their quantification allows system designers to assess its security. Various measures of power system resilience have been investigated throughout literature. For instance, the average efficiency of the network [1], adapted to the case of the North American power grid, is used by [2] to quantify the performance of grid operations before and after the occurrence of breakdowns. This measure is based on the most efficient path between the generation substation i and the distribution substation j, where path efficiency between two nodes i and j is the harmonic composition of the efficiencies of the component edges. Then, the damage caused by a failure is defined as the normalized efficiency loss.

The duration of unscheduled outages due to failure of distribution system (i.e., excluding outages due to failure of generation or transmission systems) is proposed in [3] as a resilience measure. The authors hypothesize that the resilience of power distribution systems depends on two main factors: one is the power distribution infrastructure (including the environment within which it operates and interactions between the two). Second factor is the priority given to restoration by the power company (including the effectiveness of the power company's response). A resilience factor and uncertainty-weighted resilience measure proposed by [4] are implemented via the set of resilience capacities: absorptive capacity, adaptive capacity, and recovery and restorative capacity. A system-level measure to quantify the resilience of smart grid is also proposed by [5], which integrates five resilience indices: expected hazard frequency, initial failure scale, maximum impact level, recovery time and recovery cost. This measure can be computed by normalizing the difference between the annual targeted performance area and the annual impact area.

Roege et al. [6] identified resilience measures to provide guidance for energy systems planning, design, investment, and operation. Recommendations are presented using a matrix format to provide a structured and comprehensive framework relevant to a system's energy resilience. Each cell within the matrix correlates how can a system's ability to [plan/prepare, absorb, recover and adapt] to an energy-related change be improved by measures taken in the [physical, information, cognitive and social] domain. A recent survey [7] summarized resilience measures of energy distribution systems. The building blocks of resilience are: *inputs* available to support resilience, *capacities*, which are the ways in which inputs are organized to support resilience, *capabilities* of what tasks can be performed, the *performance* and *outcomes* that describe what is produced by an engineered system. These building blocks address the goal of reducing the damage from disasters.

The main contribution of this paper is to introduce the notion of Level-of-Resilience (LoR) as a way to compare the resiliency of different systems, subject to various attack scenarios. An adverse event can affect both system's stability and performance, and whose recovery time is also another important metric. Accordingly, in our present work, we consider size of Region-of-Stability (RoS), the Level-of-Performance (e.g., load served in case of a power system), and Recovery-Time as part of resilience metric. When subjected to adverse events, the *RoS* evolves under attack and recovery actions which we capture as a "*modal-RoS*". This evolution of RoS is computed following the approach of [8] based on level set reachability analysis. This, along with the Level-of-Performance-Reduction (LoP_R), due to system attacks and as measured in terms of percentage of reduction of load served, and the *Recovery-time (RT)* from faults/attacks are used to compare the Level-of-Resilience (LoR).

II. Power System Dyamics and Transient Stability to Large Disturbances

A power system consists of: (i) generator (PV) buses, for which generator real power and voltage magnitude are specified, (ii) load (PQ) buses, for which real and reactive load powers are specified, and occasionally (iii) a slack bus, for which the voltage magnitude and phase are specified (typically zero phase is used, making this bus as a reference). The dynamics at a generator bus can be modeled by a pair of differential equations that are referred to as the swing equations [9]. The swing equations for generator i in an interconnected power system are expressed as:

$$\dot{\delta}_i = \omega_i \tag{1}$$
$$M_i\dot{\omega}_i = -D_i\omega_i + P_{m,i} - P_{e,i} \qquad i = 1, ...n, \tag{2}$$

where the electrical power of generator i satisfies:

$$P_{e,i} = \sum_{j=1}^{n} |E_i| \times |E_j| \times [G_{ij}\cos(\delta_i - \delta_j) + B_{ij}\sin(\delta_i - \delta_j)], \tag{3}$$

In (1), (2), M_i is inertia constant; D_i is damping constant, $P_{m,i}$ is mechanical power input; $P_{e,i}$ is the electrical power output; δ_i is angle of internal complex voltage of i^{th} machine; and ω_i is rotor angle velocity of the i^{th} machine with respect to the reference frequency of the power system

This research was supported in part by PNNL and John Deere through NSF-IUCRC, Security and Software Engineering Research Center (S2ERC), and the National Science Foundation under the grants NSF-CCF-1331390 and NSF-ECCS- 1509420. [1] Jun Chen is now with Idaho National Laboratory upon graduation from ISU.

978-1-5090-4190-9/16/$31.00 ©2016 IEEE

ω_r. In (3), E_i is i^{th} machine's internal complex voltage; $G_{ij} = G_{ji} \geq 0$ is the Kron-reduced equivalent conductance between generator i and generator j; $B_{ij} = B_{ji} > 0$ is the Kron-reduced equivalent susceptance between generator i and generator j, and $Y_{ij} = G_{ij} + \sqrt{-1}B_{ij}$ is the Kron-reduced equivalent admittance between generator i and generator j (the ij^{th} element of Kron-reduced equivalent admittance matrix Y_I of size $|n| \times |n|$). The solution of (1)-(3) in steady state yields the so called *power flow solutions* that yield the magnitude and phase angle of the voltage at each bus, and the power flowing in each line.

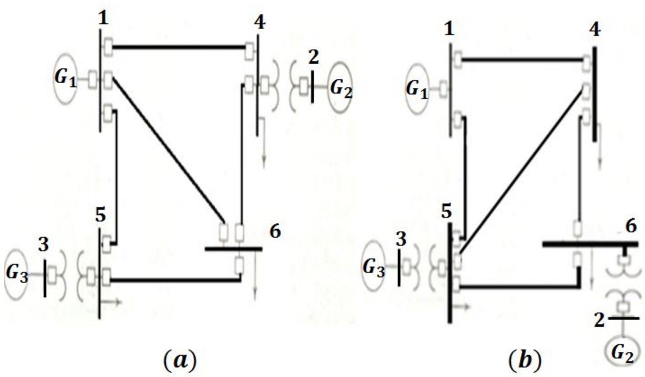

Fig. 1. (a) System PS_1, and (b) System PS_2.

For the sake of illustration, we consider a pair of power systems with identical buses, generators and loads but with different topologies, as shown in Fig. 1. For the 1^{st} power system, PS_1, bus 1 is the *slack* bus, buses 2 and 3 are the generator buses, and buses 4, 5, and 6 are the load buses. The machine, load and line data, generation schedule, and reactive power limits for the regulated buses, along with power flow solution data for PS_1 are tabulated in Appendix, Tables III-VII. The 2^{nd} power system, PS_2, has same generation and loads as PS_1, but with different topology, where line L_{16} appears as line L_{45}. PS_2 data are also given in Appendix, Tables III-VIII. We show that while the two systems are served by the same generators, and serve the same set of loads, they have different resiliency to the same attacks owing to their topological difference.

III. Level-of-Resilience Formulation

A. Modal-RoS and Region-of-Stability-Reduction

For a nonlinear autonomous system, the stability region is defined as the set of all initial points from which the autonomous system eventually converges to a stable-equilibrium-point (SEP) [10]. For the simplicity of discussion, we assume that the system is lossless, so the transfer admittance is purely imaginary [11].

Define an energy function $V(\vec{\delta}, \vec{\omega})$, where $\vec{\delta} = [\delta_1, \ldots, \delta_n]^T$ and $\vec{\omega} = [\omega_1, \ldots, \omega_n]^T$, as follows:

$$V(\vec{\delta}, \vec{\omega}) = \frac{1}{2}\sum_{i=1}^{n} M_i \omega_i^2 - \sum_{i=1}^{n} P_{m,i}\delta_i - \sum_{i=1}^{n}\sum_{j=i}^{n} |E_i| \times |E_j| \times [B_{ij}\cos(\delta_i - \delta_j)]. \quad (4)$$

The dissipative nature of the damping term in (2) ensures that the energy constructed in this way is always decreasing in time.

Using the potential energy function, the swing equations (1), (2) can be rewritten as follows:

$$\dot{\delta}_i = \omega_i \quad (5)$$

$$\dot{\omega}_i = \frac{1}{M_i}[-D_i\omega_i - \frac{\partial V_P}{\partial \delta_i}(\vec{\delta})]. \quad (6)$$

A point $(\vec{\delta}^e, 0)$ is an equilibrium of (5) and (6) if and only if $(\partial V_P/\partial\vec{\delta})(\vec{\delta}^e) = 0$. Since $\vec{\omega}^e = 0$, the energy function at the equilibrium is of form: $V(\vec{\delta}^e, \vec{\omega}^e) = V_P(\vec{\delta}^e)$ [12], [13]. Then, the stability region of a power system can be equivalently studied in the $\vec{\delta}$ subspace.

$$\dot{\vec{\delta}} = -\frac{\partial V_P}{\partial \vec{\delta}}(\vec{\delta}). \quad (7)$$

The stability boundary of (7) is the potential energy boundary surface of (5), (6).

For RoS computation, given a SEP $\vec{x}^e$ of a system, we propagate in time the boundary of the backward reachable set of $\vec{x}^e$, i.e., the set of states starting from where trajectories can reach the SEP, by solving the following *Hamilton-Jacobi-Isaacs* (HJI) PDE:

$$\phi_{\vec{x}}^T f(\vec{x}) + \phi_t = 0. \quad (8)$$

This PDE describes the propagation of the backward reachable set boundary, specified by $\phi(\vec{x}, t) = 0$, as a function of time, in which $\phi_{\vec{x}}^T = [\frac{\partial\phi}{\partial x_1}, ..., \frac{\partial\phi}{\partial x_n}]$, and with terminal conditions:

$$\phi(\vec{x}, 0) = ||\vec{x} - \vec{x}^e|| = 0.$$

The backward reachable set of the SEP $\vec{x}^e$ (computed using the toolbox of level set methods [14]) is always contained in the region of stability of the SEP $\vec{x}^e$, and as t goes to infinity, the backward reachable set approaches the true region of stability.

Owing to the presence of protective relays that enact disconnection of any faulted circuits, the power system under fault undergoes configuration changes in three stages, from pre-fault, faulted, to post-fault systems. The pre-fault system will inhabit a known initial stable equilibrium. When a large disturbance/fault occurs at a time t_f, the system transitions to the faulted condition before it is cleared at time t_c by the protective system operation. The *critical clearing time*, denoted as t_c^*, is the largest value of t_c, so, the post-clearance system with initial condition $\vec{x}(t_c)$ will converge to a stable equilibrium point.

A modal-Region-of-Stability "*modal-RoS*" is a graphical representation that captures the evolution of RoS through the changes of systems modes of configurations under a sequence of fault and recovery actions. We denote a *modal-RoS* for a given sequence of fault and recovery actions as: $RoS_I \rightarrow RoS_{P1} \rightarrow ... \rightarrow RoS_{Pm}$, where I is the initial pre-fault configuration mode, "$\rightarrow$" designates mode change, and $P1, ..., Pm$ are the new post-fault configuration modes as a sequence of m fault and recovery actions take place sequentially in time. Fig. 3(a) shows RoS evolution for PS_1 from its pre-fault mode I; its state trajectory when fault is applied at line L_{15} causing RoS to be lost is shown in Fig. 3(b); post-fault Region-of-Stability RoS_{P1} in Fig. 3(c); and post-fault state trajectory within RoS_{P1} when clearance is applied within critical time in Fig. 3(d). Then, repeating this process for a sequence of fault and recovery actions, a *modal-RoS* can be generated. Fig. 2 shows an attack scenario A_1 in which three lines are faulted in the sequence: $L_{15} \rightarrow L_{46} \rightarrow L_{56}$, interleaved with recovery actions. Accordingly, the *modal-RoS*: $RoS_I \rightarrow RoS_{P1} \rightarrow RoS_{P2}$, is shown in Fig.

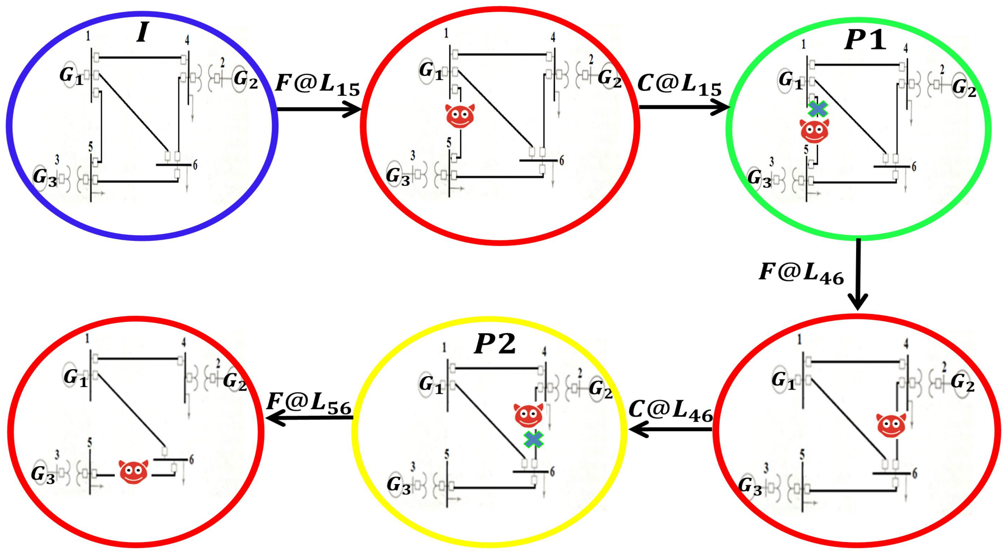

Fig. 2. PS_1 topology evolution under A_1 (transition label F denotes fault, whereas C denotes its clearance).

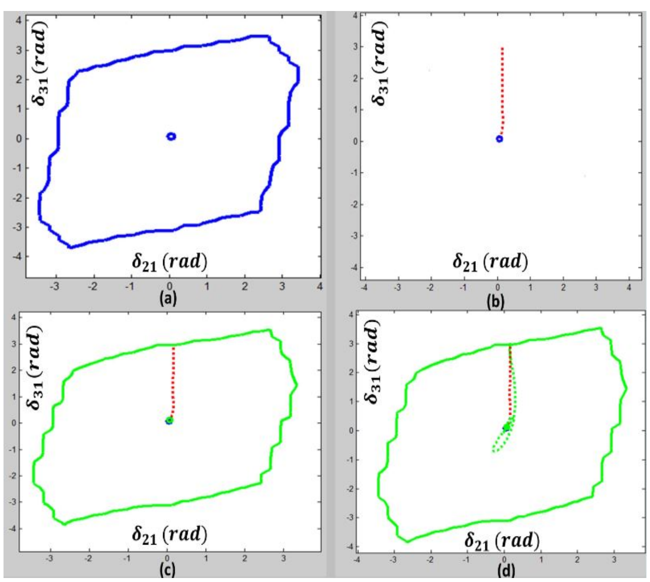

Fig. 3. PS_1 RoS evolution (a) pre-fault RoS_I; (b) state trajectory when fault occurs at line L_{15}; (c) RoS_{P1} for mode $P1$ after fault is cleared; (d) post-fault state trajectory within RoS_{P1} when fault is cleared within critical time.

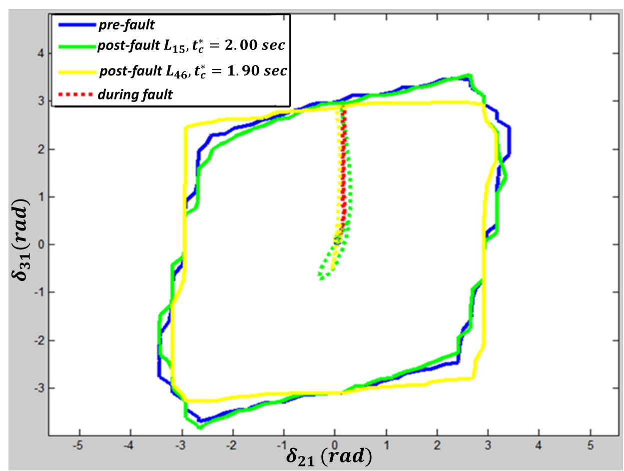

Fig. 4. PS_1 *modal-RoS* under A_1.

4, where $P1$ is post-fault mode after clearing line L_{15} fault, and $P2$ is post-fault mode after line L_{46} fault is cleared. Note the RoS is lost after the final L_{56} fault, and so *modal-RoS* terminates at this fault.

Definition 1. *Given a modal-RoS: $RoS_I \rightarrow RoS_{P1} \rightarrow \ldots \rightarrow RoS_{Pm}$, the percentage of RoS-Reduction, RoS_R, is given by,*

$$RoS_R = \frac{D_I - D_{Pm}}{D_I}\%, \tag{9}$$

where for a given RoS boundary Ω in n-dimensional space with equilibrium $\vec{x}^e$, D can be computed as the shortest Euclidean distance between Ω and $\vec{x}^e$:

$$D = min_{\vec{q}\in\Omega}||\vec{q} - \vec{x}^e|| = min_{\vec{q}\in\Omega}\sqrt{\sum_{k=1}^{n}(q_k - x_k^e)^2}. \tag{10}$$

B. Level-of-Performance-Reduction

Associated with each *modal-RoS* is a Level-of-Performance-Reduction (LoP_R), measured as the percentage of reduction of load served along the various modes of the *modal-RoS*.

Definition 2. *Given a modal-RoS: $RoS_I \rightarrow RoS_{P1} \rightarrow \ldots \rightarrow RoS_{Pm}$,*

Level-of-Performance-Reduction, LoP_R, is defined as:

$$LoP_R = \frac{\sum_{\text{loads in mode } I} p_{\text{real}} - \sum_{\text{loads in mode } Pm} p_{\text{real}}}{\sum_{\text{loads in mode } I} p_{\text{real}}}\%.$$

C. Level-of-Resilience

Level-of-Resilience (LoR) is determined by comparing the RoS_R, and also the LoP_R, as measured along the various modes of the *modal-RoS*. (For the moment, we ignore Recovery Time since this is the same for the two power systems.) For a given attack scenario, we compute the LoR as follows. First for the initial pre-fault mode I, compute the RoS of its SEP $\vec{x}_I^e$. For any perturbation/low level disturbance (e.g., transient change in load) that does not switch the mode, the perturbed state must be within the RoS of the pre-fault system for the system to remain stable (state trajectory still converge to $\vec{x}_I^e$). When a fault/severe disturbance occurs affecting the system structure, a new Kron-reduced equivalent admittance matrix Y_F corresponding to faulted mode is generated; the system may become unstable without any recovery action rendering the RoS to be an empty set. The fault can be cleared by isolating the faulted line using circuit breakers. If the fault is not cleared within a critical time window (t_c^*), then overall system might no longer be stable. When fault is cleared within the critical time, a new kron reduced admittance matrix Y_P is obtained, corresponding to post-fault mode P. The system will stabilize to a new equilibrium point $\vec{x}_P^e$ of mode P only if the forward reachable state trajectory under fault starting from pre-fault $\vec{x}_I^e$ $, i.e., Reach_f^+(\vec{x}_I^e)$ is within the RoS of $\vec{x}_P^e$. This is captured by the requirement:

$$t_c \text{ such that } Reach_f^+(\vec{x}_I^e, t_c) \in RoS(\vec{x}_P^e).$$

Such pre-fault and post-fault RoSs can continue to be sequenced for any subsequent attacks to yield a sequence of RoSs, a *modal-RoS*. Associated with each RoS is a Level-of-Performance-Reduction (LoP_R), measured as the percentage of reduction of load served. Using the size of RoS and the associated LoP_R for the eventual mode, we can measure and compare Level-of-Resilience (LoR). Another aspect of resiliency metric is *Recovery-Time (RT)*, which is the time system takes to detect and recover from an attack or a fault.

Definition 3. *Given two systems PS_1, PS_2, and an attack scenario A, $LoR(PS_1, A) > LoR(PS_2, A)$ if:*
$[RoS_R(PS_1, A) < RoS_R(PS_2, A)]$
$\vee$ $[[RoS_R(PS_1, A) = RoS_R(PS_2, A)] \wedge [LoP_R(PS_1, A) < LoP_R(PS_2, A)]]$
$\vee$ $[[RoS_R(PS_1, A) = RoS_R(PS_2, A)] \wedge [LoP_R(PS_1, A) = LoP_R(PS_2, A)] \wedge [RT(PS_1, A) < RT(PS_2, A)]]$.

In power systems, local controls are used for detection and clearance of faults, and so RT is typically independent of system topology and hence not included in Definition 3, but could be included for general dynamical systems.

IV. Experimental Comparison of *LoR*

In this section, we simulate two different attack scenarios for two different power systems PS_1 (Fig. 1(a)) and PS_2 (Fig. 1(b)), with same generators and loads, but with different topology, and for each scenario we evaluate and compare their LoR. In order to simplify the transient stability analysis for the purposes of our example, assumptions are made as follows (similar assumptions can be found in [15], [9]): each synchronous machine is represented by a constant voltage source behind the direct axis transient reactance. The governors actions are neglected and the input powers are assumed to remain constant during the entire period of a single mode. All loads are converted to equivalent admittances to ground and are assumed constant.

Consider the first attack scenario A_1, in which three lines are faulted in the sequence: $L_{15} \rightarrow L_{46} \rightarrow L_{56}$. For PS_1,

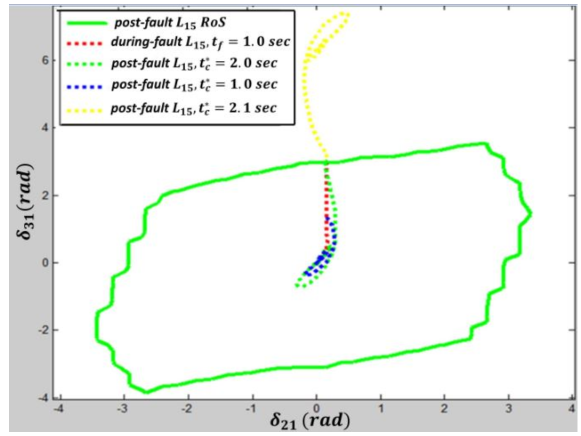

Fig. 5. PS_1 post-fault RoS when fault is applied at 1 sec at L_{15} and state trajectories under several clearance times.

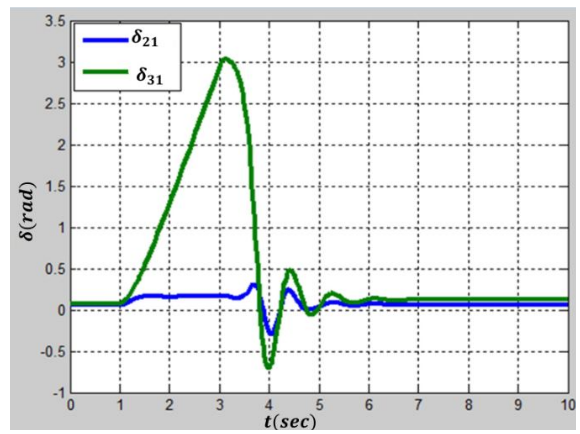

Fig. 6. PS_1 relative angles when fault is applied at 1.0 sec, and t_c^* = 2.0 sec.

the initial pre-fault equilibrium angles are: $(0.0560, 0.0783)$ rad. Three phase fault is applied at line L_{15} near bus 5 at time 1 sec, and cleared by the simultaneous opening of breakers at both ends of the line. The critical time is obtained by observing system trajectories under different clearance times so that the system angles after clearance converge to post-fault steady state equilibrium point $(0.0643, 0.1202)$, as shown in Fig. 5. This is also observed in actual behavior as shown in Fig. 6. For the L_{15} fault, the critical clearance time, t_c^* is near 2.00 sec.

Next, a second fault is applied at line L_{46} near bus 6 at time 11 sec, and later cleared by the simultaneous opening of breakers at both ends of this line. The new post-fault equilibrium point is $(0.0584, 0.1381)$, and t_c^* is near 1.90 sec. If we apply a third fault at line L_{56} near bus 5 at time 21 sec, then, regardless of the clearance time, machine 3 no longer runs in synchronism (i.e., its relative angle diverges). Fig. 7 shows the corresponding relative angles under A_1. Fig. 4 shows the evolution of RoS for PS_1, yielding a *modal-RoS* as discussed earlier.

We simulate the same attack sequence A_1 for the second power system, PS_2, shown in Fig. 1(b). Initial pre-fault equilibrium angles are: $(-0.0204, 0.0578)$ rad. A three phase fault is applied at line L_{15} near bus 5 at time 1 sec, with $t_c^* = 1.62$ sec, and post-fault equilibrium $(-0.0050, 0.0810)$. Next a second fault is applied at line L_{46} near bus 6 at time 11 sec, and cleared within $t_c^* = 2.09$ sec, with post-fault equilibrium at $(-0.0137, 0.0765)$. Finally, applying a third

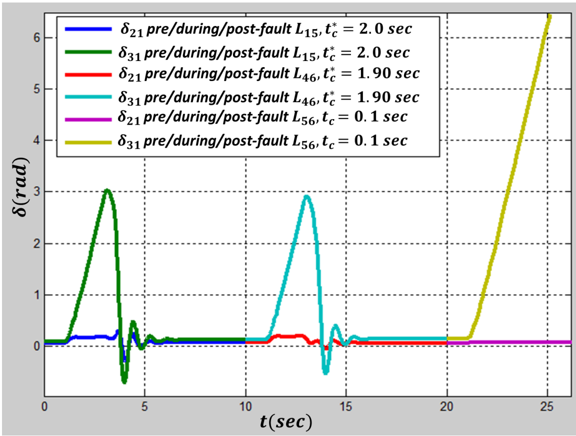

Fig. 7. PS_1 relative angles under A_1.

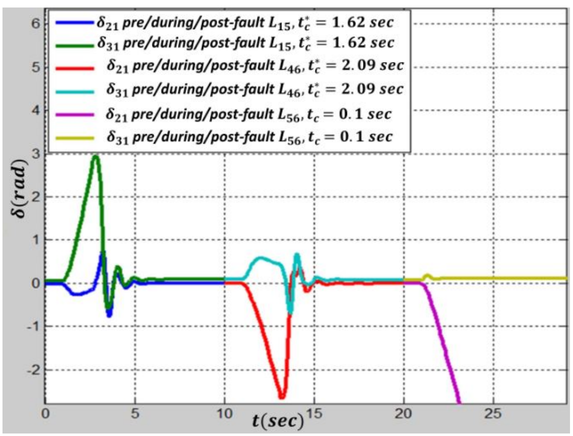

Fig. 8. PS_2 relative angles under A_1.

fault at line L_{56} at time 21 sec causes machine 2 to fall out of synchronism, regardless of the clearance time. Fig. 8 shows the system relative angles with respect to time. Fig. 9 shows the RoS evolution for PS_2, yielding its own *modal-RoS*.

For PS_1 (respectively, PS_2), the protective relay elements across machine 3 (respectively, machine 2) would interpret the loss of synchronizing condition as an abnormal operating condition and trip machine 3 (respectively, machine 2) [16], ensuring its protection. In the end, PS_1 has Level-of-Performance-Reduction, $LoP_R = 25.71\%$, while for PS_2, $LoP_R = 45.71\%$.

For comparing LoR of PS_1 and PS_2, under attack scenario A_1, Table I shows the nearest distance from equilibrium to boundary associated with each RoS, as well as RoS_R. PS_2 has higher RoS_R (15.018%) as opposed to PS_1 (4.507%). Also, $LoP_R(PS_1, A_1) < LoP_R(PS_2, A_1)$. Hence, $LoR(PS_1, A_1) > LoR(PS_2, A_1)$. Thus, PS_1 is more resilient to attack scenario A_1 as compared to PS_2.

TABLE I
SIZE OF EACH RoS (rad) AND $RoS_R(\%)$ UNDER A_1

A_1 :	D_I	$D_{P(L_{15})}$	$D_{P(L_{46})}$	RoS_R
PS_1	2.840	2.712	2.712	4.507
PS_2	2.710	2.374	2.303	15.018

Similarly, under another attack scenario, $A_2 : L_{56} \rightarrow L_{14} \rightarrow L_{46}$, *modal-RoS* for PS_1 (respectively, PS_2) are shown in Fig. 10 (respectively, Fig. 11).

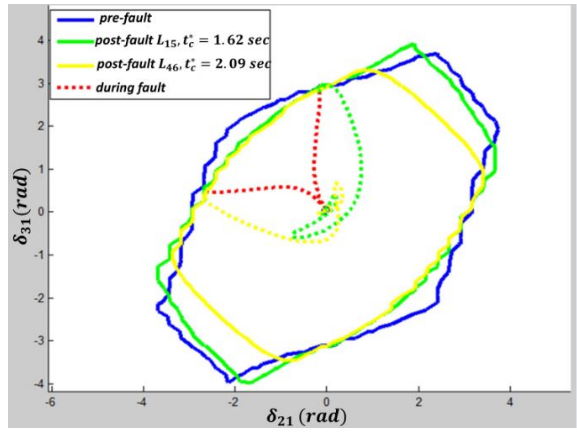

Fig. 9. PS_2 *modal-RoS* under A_1.

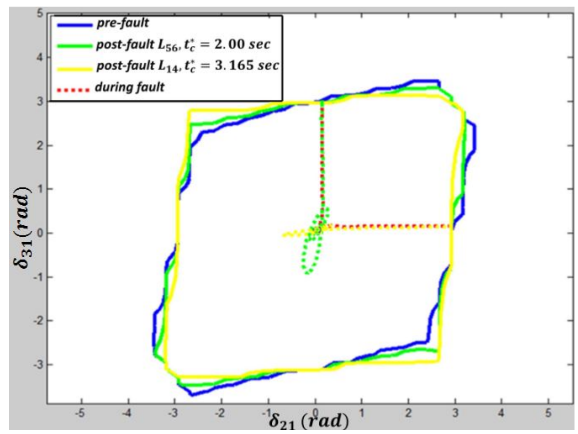

Fig. 10. PS_1 *modal-RoS* under A_2.

Table II shows the nearest distance between equilibrium and boundary associated with each RoS, as well as RoS_R. PS_2 has higher RoS_R (0.996%) as opposed to PS_1 (−0.634%). Also, for PS_1, $LoP_R = 28.57\%$, while for PS_2, $LoP_R = 45.71\%$, so $LoR(PS_1, A_2) > LoR(PS_2, A_2)$, implying that topology PS_1 is more resilient as compared to PS_2, under both the attack scenarios.

TABLE II
SIZE OF EACH RoS (rad) AND $RoS_R(\%)$ UNDER A_2

A_2 :	D_I	$D_{P(L_{56})}$	$D_{P(L_{14})}$	RoS_R
PS_1	2.840	2.878	2.858	-0.634
PS_2	2.710	2.776	2.683	0.996

V. Conclusion

In this work, we proposed a measure for comparing Level-of-Resilience (LoR) for power systems. This measure is based on comparing systems characteristics: percentage of Region-of-stability-Reduction (RoS_R), percentage of Level-of-Performance-Reduction (LoP_R), and the system recovery-time, under the given attack scenarios. The system state trajectories and RoS evolution are tracked and captured in form of *modal-RoS*. Examples were illustrated to compare the LoR of two different power system topologies under two different attack scenarios. While the results were employed for power systems, they more generally apply to any hybrid

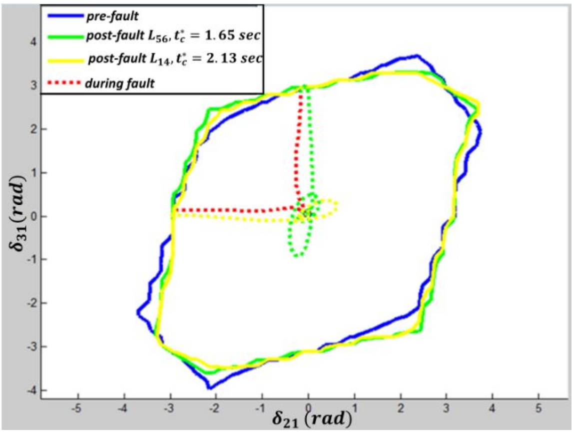

Fig. 11. PS_2 *modal-RoS* under A_2.

dynamical system with both continuous and discrete dynamics, where the discrete state changes (i.e., mode switches) are caused by attack and/or recovery actions. A note about *recovery time*, within which a recovery action can be taken, is that for power systems it corresponds to the time taken to detect and clear faults, which does not vary dramatically from one system topology to another, and so not considered explicitly in the resiliency comparison measure of our example. For general hybrid dynamical systems, however, recovery time can also be included in the comparison measure. The work presented here provides a framework to do so. Also, for the general adoption of the approach, one must further provide computationally efficient tool for LoR comparison, and this can be a subject of further study. One could also consider a simplified metric for measuring level of stability such as *stability margin*, which is easier to compute than for example region-of-stability.

Appendix

In this appendix, we provide the modeling data for the power systems PS_1 and PS_2 that we use as running examples.

TABLE III
MACHINE DATA FOR BOTH PS_1 AND PS_2

Gen.	$R_a(PU)$	$X_d(PU)$	M(sec^2/rad)	D(sec/rad)
1	0	0.2	0.106	0.12
2	0	0.15	0.021	0.12
3	0	0.25	0.027	0.12

TABLE IV
GENERATION SCHEDULE FOR BOTH PS_1 AND PS_2

Bus No.	Voltage(Mag.)	Generation(MW)	Qmin.(Mvar)	Qmax.(Mvar)
1	1.06	0		
2	1.04	150	0	140
3	1.03	100	0	90

TABLE V
LOAD DATA FOR BOTH PS_1 AND PS_2

Bus No.	Load(MW)	Load(Mvar)
1	0	0
2	0	0
3	0	0
4	100	70
5	90	30
6	160	110

TABLE VI
LINE DATA FOR PS_1 (AND PS_2 WITH REORDERING)

Bus No.	Bus No.	R(PU)	X(PU)	$(1/2B)(PU)$
1	4	0	0.225	0.0065
1	5	0	0.105	0.0045
1	6	0	0.215	0.0055
2	4	0	0.035	0.0000
3	5	0	0.042	0.0000
4	6	0	0.125	0.0035
5	6	0	0.175	0.0300

TABLE VII
POWER FLOW SOLUTION FOR PS_1

Bus No.	Voltage (Mag.)	Angle (Degree)	Load(MW)	Load(Mvar)	Generation(Mw)	Generation(Mvar)
1	1.060	0.000	0.000	0.000	100.000	116.170
2	1.040	1.217	0.000	0.000	150.000	97.704
3	1.030	0.412	0.000	0.000	100.000	27.919
4	1.008	-1.653	100.000	70.000	0.000	0.000
5	1.019	-1.881	90.000	30.000	0.000	0.000
6	0.960	-6.368	160.000	110.000	0.000	0.000

TABLE VIII
POWER FLOW SOLUTION FOR PS_2

Bus No.	Voltage (Mag.)	Angle (Degree)	Load(MW)	Load(Mvar)	Generation(Mw)	Generation(Mvar)
1	1.060	0.000	0.000	0.000	100.000	82.304
2	1.040	-2.391	0.000	0.000	150.000	125.447
3	1.030	-0.370	0.000	0.000	100.000	26.545
4	0.977	-6.511	100.000	70.000	0.000	0.000
5	1.020	-2.661	90.000	30.000	0.000	0.000
6	0.999	-5.287	160.000	110.000	0.000	0.000

References

[1] V. Latora and M. Marchiori, “Efficient behavior of small-world networks,” *Physical Review Letters*, vol. 87, no. 19, p. 198701, Oct. 2001.

[2] R. Kinney, P. Crucitti, R. Albert, and V. Latora, “Modeling cascading failures in the north american power grid,” *The European Physical Journal B*, vol. 46, pp. 101–107, Aug. 2005.

[3] P. J. Maliszewski and C. Perrings, “Factors in the resilience of electrical power distribution infrastructures,” *Applied Geography*, vol. 32, pp. 668–679, 2012.

[4] R. Francis and B. Bekera, “A metric and frameworks for resilience analysis of engineered and infrastructure systems,” *Reliability Engineering and System Safety*, vol. 121, pp. 90–103, 2014.

[5] M. Ouyang and L. Due$\tilde{n}as-$Osorio, “Resilience modeling and simulation of smart grids,” *Structures Congress ASCE*, 2011.

[6] P. E. Roege, Z. A. Collier, J. Mancillas, J. A. McDonagh, and I. Linkov, “Metrics for energy resilience,” *Energy Policy*, vol. 72, pp. 249–256, 2014.

[7] H. H. Willis and K. Loa, “Measuring the resilience of energy distribution systems,” *RAND Corporation, Santa Monica, Calif.*, 2015.

[8] L. Jin, R. Kumar, and N. Elia, “Reachability analysis based transient stability design in power systems,” *Electrical Power and Energy Systems*, vol. 32, no. 7, pp. 782–787, Jan. 2010.

[9] M. A. Pai, *Energy Function Analysis for Power System Stability*. Kluwer academic publishers, 1989.

[10] H. K. Khalil, *Nonlinear Systems*, 3rd ed. Prentice Hall, 2002.

[11] C.-W. Liu and J. S. Thorp, “A novel method to compute the closest unstable equilibrium point for transient stability region estimate in power systems,” *IEEE Trans. Circuits and Systems-I: Fundamental Theory and Applications*, vol. 44, no. 7, pp. 630–635, Jul. 1997.

[12] H.-D. Chiang, F. F. Wu, and P. P. Varaiya, “Foundations of direct methods for power system transient stability analysis,” *IEEE Trans. on Circuits and Systems*, vol. Case-34, no. 2, pp. 160–173, Feb. 1987.

[13] R. J. Thomas and J. S. Thorp, “Towards a direct test for large scale electric power system instabilities,” in *Proc. 24th Conference on Decision and Control*, Lauderdale, FL, Dec. 1985, pp. 65–69.

[14] I. Mitchell. A toolbox of level set methods version 1.0. [Online]. Available: http://www.cs.ubc.ca/ mitchell/ToolboxLS/

[15] H. Saadat, *Power System Analysis*. McGraw-Hill Education, 1999.

[16] M. J. Thompson, “Fundamentals and advancements in generator synchronizing systems,” in *Proc. the 65th Annual Conference for Protective Relay Engineers*, College Station, TX, Apr. 2012, pp. 203–214.